IEEE Access
Multidisciplinary | Rapid Review | Open Access Journal

Received March 26, 2020, accepted April 22, 2020, date of publication April 24, 2020, date of current version May 7, 2020.

Digital Object Identifier 10.1109/ACCESS.2020.2990349

Regenerative Braking Control Strategy for Electric Vehicles Based on Optimization of Switched Reluctance Generator Drive System

YUEYING ZHU[1], (Member, IEEE), HAO WU[1], AND JUNXIA ZHANG[1,2]

[1]College of Mechanical Engineering, Tianjin University of Science and Technology, Tianjin 300222, China
[2]Tianjin Key Laboratory of Integrated Design and On-line Monitoring for Light Industry & Food Machinery and Equipment, Tianjin 300222, China

Corresponding author: Yueying Zhu (zhuyueying@tust.edu.cn)

This work was supported in part by the National Key Research and Development Program of China under Grant 2016YFD0701000, and in part by the National Natural Science Foundation of China under Grant 51505332.

ABSTRACT To improve braking performance and regenerative energy of front drive electric vehicles (EVs) driven by switched reluctance motor (SRM), a regenerative braking control strategy based on multi-objective optimization of switched reluctance generator (SRG) drive system is proposed in this paper. Firstly, a partition braking force distribution strategy is developed by jointly considering braking energy and safety, and SRG drive system model is established based on low and high-speed condition. The vehicle braking system model including mechanic and regenerative braking system is built. Then, a multi-objective optimization function with three weight factors is defined, where output generated power, torque smoothness, and current smoothness are selected as optimization objectives to improve the driving range, braking comfort, and battery lifetime, respectively. Furthermore, a multi-objective optimization controller with variable switch angles is designed and combined with vehicle braking system. Finally, braking energy recovery efficiency, braking smoothness, and charging current smoothness under the multi-objective optimization controller for SRG are analyzed and compared with those under output power optimization controller. The comparison results show that the regenerative braking control strategy based on multi-objective optimization of SRG can effectively increase the vehicle braking comfort and improve battery lifetime without decreasing recovery energy.

INDEX TERMS Electric vehicle, switched reluctance generator, braking force distribution, multi-objective optimization.

I. INTRODUCTION

Environmental pollution and energy shortages have accelerated the development and use of green renewable energy. Electric vehicle (EV) has advantages of low pollution, low noise, and high energy efficiency, which has become the focus of research in the automotive industry [1]–[3]. Currently, switched reluctance motor (SRM) is considered as one of the best options for driving EVs because of its advantages of simple structure, low cost, high reliability, large power generation, and high efficiency in a wide speed range [4]–[6]. Meanwhile, the traction system with SRM can also recover more energy during condition of regenerative braking. However, SRM has the disadvantage of high torque ripple [7], [8], which will directly affect the vehicle braking comfort and stability. In addition, the energy recovery efficiency and the charging current of the switched reluctance generator (SRG), which imply driving range and battery lifetime of EV, respectively, are hard to be synthetically improved for EVs due to the SRG characteristics of complex generating principle [9], [10].

In order to increase the driving range of EVs, braking system in EV is generally combined by mechanical braking and regenerative braking [11]. In recent years, to improve the braking system performance of EVs, a host of research has been carried out in the fields of energy management of EVs [12]–[14], emergency braking control strategies [15], and anti-lock braking system (ABS) [16]. Besides, the coupling control for mechanical and regenerative braking force was also researched to improve the braking

The associate editor coordinating the review of this manuscript and approving it for publication was Xiaosong Hu.

performance. A new regenerative braking system scheme was put forward to ensure the maximum regenerative braking force in [17]. In [18], a segmented front and rear wheel braking force distribution control strategy was proposed to recover braking energy as much as possible on the premise of ensuring braking safety. A new regenerative braking control strategy based on ideal braking force distribution strategy was presented to improve the regeneration efficiency in [19]. And [20] proposed a novel regenerative braking system scheme to improve energy efficiency and extend the driving distance of EVs. In comparison to other solutions, the novel solution has better performance in robustness, and efficiency. In addition, to solve the problem of vehicle lateral stability caused by the transition from regenerative braking to hybrid braking, a coordinated distribution control strategy was proposed in [21]. However, the above studies concentrate on braking force coupling control strategies to ensure the maximum regenerative braking force, generate the maximum possible energy, or achieve braking stability of EVs, without considering the effects of nonlinear dynamic characteristics of electric motors on the vehicle braking system. Furthermore, a multitude of research has been carried out recently aiming at generating control strategies of SRG drive system. In [22], a method for optimizing SRG using two forms of direct power control (DPC) at a wide speed range was proposed to make mechanical energy well captured. In [23], a maximum power point tracking (MPPT) strategy was presented to maximize the power extraction. Besides, a lot of research has been also done in restraining current fluctuation and increasing power generation efficiency for SRG. A power converter and a smart search control (SSC) approach were proposed to reduce the current fluctuation when the output power was maximum in [25]. In [24], a switching angle control strategy was proposed, which can maximize the power generation efficiency and reduce the current fluctuation. In [4], a new control strategy was proposed to minimize the current fluctuation through the control parameters, thereby maximizing the efficiency indirectly. Reference [26] presented an advanced multi-objective power flow control method to restrain battery current fluctuation. On the other hand, a novel proportional integrator current chopping control (PICCC) was presented, which can minimize the torque ripple of the SRG in [27]. Reference [6] presented modified toque ripple minimization algorithm of a four-phase 8/6 poles SRG using artificial neural network (ANN) control. A non-unity torque sharing function (TSF) was proposed to minimize the torque ripple over a wide speed range of operation for SRG in [28]. Nonetheless, the above was to improve the power generation, restrain the current fluctuation, or reduce torque ripple through various control strategies of SRG. But these indices mentioned should be selected based on system requirements and considered to be optimized comprehensively. Besides, these strategies could not be applied on EVs, because they were only proposed for SRG, instead of considering the actual requirements and dynamic characteristics of EVs.

To consider the effects of nonlinear dynamic characteristics of the motor and improve the comprehensive performance of EVs driven by SRG during braking, a regenerative braking control strategy based on multi-objective optimization of SRG drive system is proposed in this paper. Furthermore, the vehicle dynamic model and braking force distribution controller are established and co-simulated with developed multi-objective optimized SRG drive system. The results show that the proposed control strategy can effectively balance power generation, torque ripple, and current fluctuation.

This paper is organized as follows: Firstly, the braking force distribution control model and SRG model are established in Section II. Then, multi-objective optimization method for SRG is proposed and performed in Section III. The switching system for reducing the switching frequency between high and low speed control modes and optimization controller of SRG are established in Section IV. Finally, the dynamic characteristics of SRG and vehicle are analyzed and compared in Section V.

II. REGENERATIVE BRAKING SYSTEM OF EVs

A. VEHICLE DYNAMIC MODEL

The vehicle driving force F_t can be computed by means of external forces under driving condition, which is shown as

$$F_t = F_f + F_w + F_i + F_j \tag{1}$$

where, F_f, F_w, F_i, and F_j are rolling resistance, air resistance, gradient resistance, and acceleration resistance, respectively.

During the braking process, the vehicle will be subjected to air resistance, rolling resistance, gradient resistance, and braking force from front and rear wheels. The balance equation can be expressed as

$$m\frac{du}{dt} = mgf\cos\alpha + \frac{1}{2}C_D A\rho u^2 + mg\sin\alpha + F_b \tag{2}$$

where, m means vehicle mass, u refers to the speed of the vehicle, F_b is the braking force of the vehicle. The braking force F_b can be divided into two components based on front and rear axles, which can be expressed as

$$F_b = F_{bf} + F_{br} \tag{3}$$

where, F_{bf} and F_{br} are the braking forces of the front and rear axles, respectively.

The vehicle parameters researched in this paper are listed in Table 1.

B. BRAKING FORCE DISTRIBUTION

The ideal braking force distribution curve, I-curve, can ensure the best stability of the vehicle braking condition. But the recovered braking energy for front drive EVs under I-curve are not satisfied, and the control of braking system under I-curve could be rather complicated. ECE regulation curve can achieve the maximum recovered braking energy for front drive EVs because of the maximum front braking force. However, the control system under ECE curve need to be high

TABLE 1. Vehicle parameters.

Parameter	Sign	Value
Vehicle mass	m	660 kg
Wheel radius	R	0.25 m
Wheelbase	L	1.62 m
Transmission ratio	i	4.5
Mass center height	h_g	0.58 m
Rolling coefficient	F	0.014
Air resistance coefficient	C_D	0.4
Ground adhesion coefficient	φ	0.7
Distance of rear axle to center	b	0.86 m
Ramp angle	α	0 Deg
Windward area	A	1.4 m^2
Motor rated voltage	U	72 V
Motor rated torque	T	25 N·m
Motor rated power	P	4 kW

precision, where it could easily exceed the limits of ECE regulation. The β_{max} curve is a simplified ECE regulation curve with fixed front and rear wheel braking ratio [29], [30].

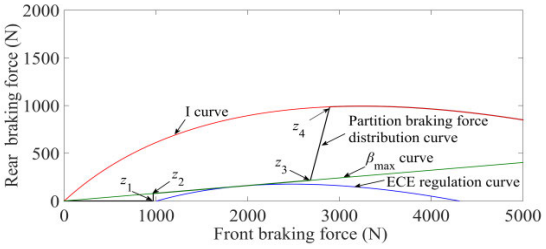

FIGURE 1. Braking force distribution curve.

When it comes to the design of braking system for EVs, the braking energy recovery should be highly considered. Therefore, the braking force distribution curve should be designed between the I-curve and ECE regulation curve [31], [32]. In this paper, a partition braking force distribution strategy is designed and applied according to braking intensity [33], where five regions are divided as shown in Fig. 1.

According to Fig. 1, the partition braking force distribution curve based on the braking intensity can be computed as

$$\begin{cases} \begin{cases} F_{bf} = mgz \\ F_{br} = 0 \end{cases}, 0 < z \le z_1 \\ \begin{cases} F_{bf} = mgz_1 \\ F_{br} = mgz - F_{bf} \end{cases}, z_1 < z \le z_2 \\ \begin{cases} F_{bf} = \beta_{\max} mgz \\ F_{br} = (1-\beta_{\max})mgz \end{cases}, z_2 < z \le z_3 \\ \begin{cases} F_{bf} = \varphi \dfrac{mg}{L}(b + zh_g) \\ F_{br} = mgz - F_{bf} \end{cases}, z_3 < z \le z_4 \\ \begin{cases} F_{bf} = z\dfrac{mg}{L}(b + zh_g) \\ F_{br} = \dfrac{1}{2}\left[\dfrac{mg}{h_g}\sqrt{b^2 + \dfrac{4h_gL}{mg}F_{bf}} - \left(\dfrac{mgb}{h_g} + 2F_{bf}\right)\right] \end{cases}, \\ \qquad z > z_4 \end{cases} \tag{4}$$

where, z represents the braking intensity.

From Fig. 1 and equation (4), it can be known that the designed partition braking force distribution curve can obtain more braking energy under the condition of medium and small braking intensity, and also ensure the braking performance in the case of high braking intensity.

C. COUPLING BRAKING FORCE CONTROL

Generally, the braking force of EVs is provided and coupled by mechanical and regenerative braking force. The regenerative braking force is limited by the maximum braking torque T_m generated by SRG, and also should be determined by considering the condition of vehicle speed u_a and the state of charge (SOC) of battery. Therefore, the influence factor k_1 for vehicle speed and the influence factor k_2 for battery SOC are proposed in this paper to adjust the regenerative braking of EVs, which can be defined as equation (5) and (6). Furthermore, the actual available maximum regenerative braking torque $T_{reg\text{-max}}$ can be calculated as equation (7).

$$k_1 = \begin{cases} 0, & u_a < 10\text{km/h} \\ 0.2(u_a - 10), & 10\text{km/h} \le u_a < 15\text{km/h} \\ 1, & u_a \ge 15\text{km/h} \end{cases} \tag{5}$$

$$k_2 = \begin{cases} 1, & SOC < 0.9 \\ 20(0.95 - SOC), & 0.9 \le SOC \le 0.95 \\ 0, & SOC > 0.95 \end{cases} \tag{6}$$

$$T_{reg\text{-max}} = k_1 k_2 T_m \tag{7}$$

For front drive EVs, the front braking force is normally generated by the mechanical braking and the regenerative braking system, while the rear braking force is provided by the mechanical braking force alone. To obtain more braking energy, the front braking force should be provided by regenerative braking system as much as possible. Therefore, the mechanical braking force distributed to front wheels can be determined by the torque required from the front wheels (T_{bf}) and the actual available maximum regenerative braking torque ($T_{reg\text{-max}}$). When the maximum regenerative braking torque provided by the motor is greater than the braking torque required by the front wheels, the front braking force can be represented by regenerative braking torque T_{reg} alone. When the maximum regenerative braking torque is less than the required front braking torque, the front braking force is jointly provided by the motor and the mechanical braking system. Under this condition, the motor outputs the maximum regenerative braking force, and the remaining front braking force is provided by the mechanical braking system. Therefore, the mechanical braking torque T_{ff} is expressed as equation (8). It should be noted when the emergency braking condition occurs, the front braking force is taken over by mechanical braking system alone to ensure braking safety. After analyzing the relationship between mechanical and regenerative braking force, the logic block diagram of coupling braking force distribution for EVs is shown in Fig. 2.

$$T_{ff} = T_{bf} - T_{reg} \tag{8}$$

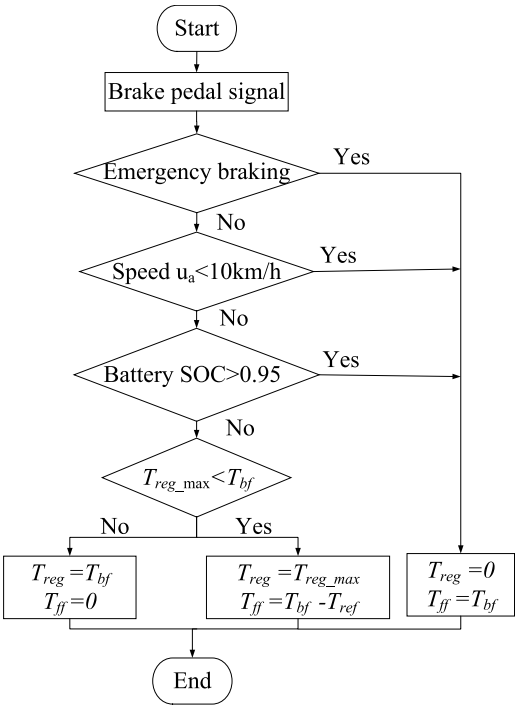

FIGURE 2. Coupling braking force control process.

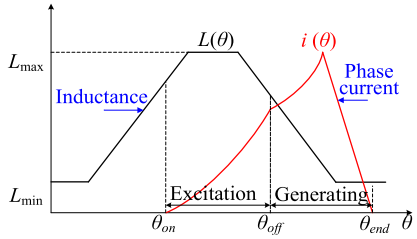

FIGURE 3. Inductance and current profile of SRG.

D. BASIC PRINCIPLE OF SRG

The SRG operating process includes two stages, which are excitation and generating period, as shown in Fig. 3. During the excitation period, one phase of SRG windings is excited by the excitation voltage, and the phase current rises. At this period, the energy is stored in the magnetic field of SRG. The SRG operates in the generating mode after excitation voltage is switched off in the descending region of the phase inductance $L(\theta)$ shown in Fig. 3. During generating period, the energy flows back to the battery. It should be noted that the current profile $i(\theta)$ shown in Fig. 3 is one of typical profiles.

Ignoring the voltage drop of the phase winding, the voltage balance equation can be obtained as follows

$$U = \frac{dL(i,\theta)i}{dt} = L(i,\theta)\frac{di}{dt} + U_E \tag{9}$$

where, U, L, i, ω, and θ are phase voltage, phase inductance, phase current, angular velocity, and rotor angle, respectively. And U_E refers to the back electromotive force (BEMF), which can be expressed as

$$U_E = i\omega\frac{dL(i,\theta)}{d\theta} \tag{10}$$

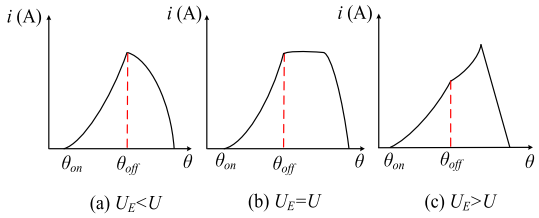

FIGURE 4. Three waveforms of phase current.

According to equation (9) and (10), various current waveforms can be obtained based on the relationship between the phase voltage U and the BEMF U_E, which are shown in Fig. 4. As shown in Fig. 4(a), the phase current decrease as soon as the accomplishment of excitation mode when BEMF U_E is lower than phase voltage U, which always happens under the condition of relatively low speed. When the rotation speed reaches a certain value, leading to $U_E = U$, the phase current will maintain a constant value for a period after the excitation mode. In this case, the rotation speed of SRG is defined as the base speed. When the speed is higher than the base speed, causing $U_E > U$, the current tends to increase first after the excitation period [20].

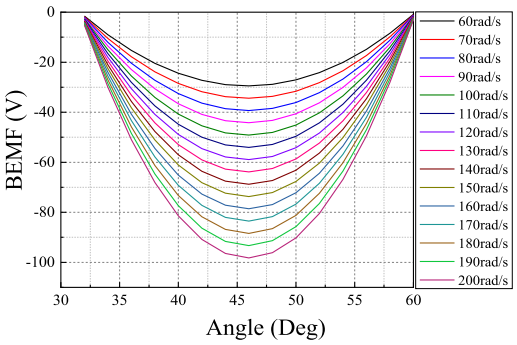

FIGURE 5. BEMF curves of SRG.

According to equation (10), The relationship of the BEMF and rotor angles under various speeds can be obtained as shown in Fig. 5. It can be seen that the base speed of the SRG in this paper is 157 rad/s (1500 r/min). Furthermore, two different control modes, current chopping control and single pulse control, are applied in this paper based on low and high speed of the SRM, respectively. The phase current profiles of the two control modes are shown in Fig. 6. It should be noted that the dynamic performance of SRG under low speed is mainly affected by three parameters, including reference current, turn-on angle, and turn-off angle. However, for high speed condition, the dynamic performance is only affected by the turn-on angle and turn-off angle.

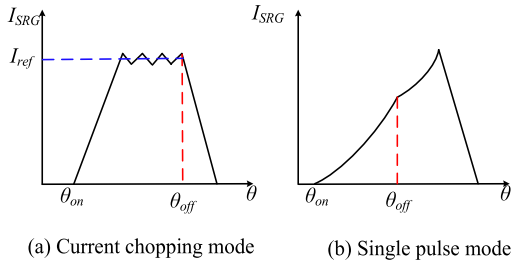

FIGURE 6. Control modes of SRG.

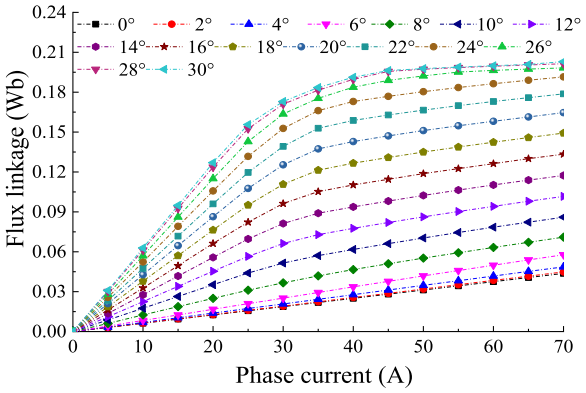

FIGURE 7. Flux linkages of the SRG.

E. SRG DRIVE SYSTEM

The dynamic characteristics of SRG cannot be well reflected by linear or quasi-linear model due to its high nonlinear characteristics [10], [34].

The flux linkages varying as position angles and phase currents are obtained by finite element method (FEM) in this paper. Meanwhile, the computing accuracy for the FEM was verified through measuring static electromagnetic characteristics of SRM in the authors' previous paper [35], [36]. Inductance and torque data are also obtained through the FEM, and the motor ontology model is established based on these data, where the flux linkage of SRG is shown in Fig. 7. The power converter and controller are also founded to constitute the SRG drive system model, which is shown in Fig. 8.

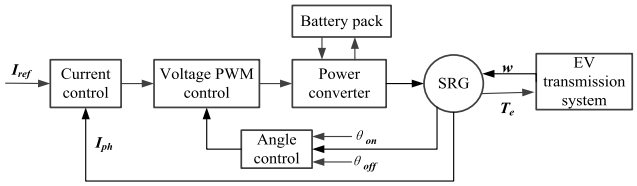

FIGURE 8. SRG drive system model.

F. THE BRAKING SYSTEM FOR EVs

As can be seen in Fig. 10, the braking system of EV is constructed, including vehicle dynamic system, braking force distribution controller, mechanical braking system, and regenerative braking system. To be specific, the mechanical braking system includes mechanical brake controller and mechanical brake actuator. The regenerative braking system is combined by motor controller, SRG, power converter, battery pack, and battery management system.

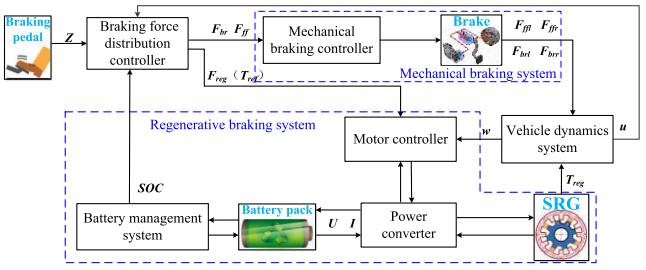

FIGURE 9. Braking system model for EVs.

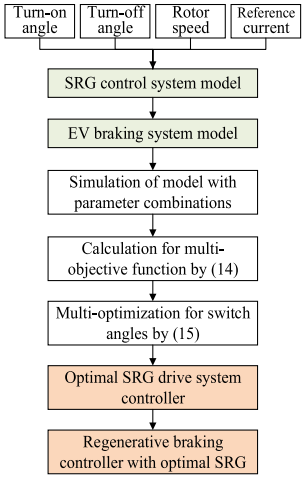

FIGURE 10. The optimization framework.

III. MULTI-OBJECTIVE OPTIMIZATION OF SRG DRIVE SYSTEM

A. SRG OPTIMIZATION OBJECTIVES

In this paper, the SRG drive system is considered for EV applications. Therefore, the desired target for optimization are higher driving range, better braking comfort, and longer battery lifetime. To optimize these targets, three optimization indexes were considered in this paper, which are power generation, torque ripple, and current fluctuation.

In order to evaluate the power generation of SRG system, the output generated power P_{out} is selected as the objective, and defined by subtracting excitation power from generating power of SRG [37], which is expressed as

$$P_{out} = P_g - P_e \tag{11}$$

where, P_g represents generating power, P_e means excitation power.

The torque smoothness τ is defined as another objective to measure the restraint degree of torque ripple, which is employed to evaluate the braking comfort performance of EVs. Generally, it could be computed by means of average

torque T_a as equation (12) according to [38].

$$\tau = \min\left\{\frac{T_a}{T_{max} - T_a}, \frac{T_a}{T_a - T_{min}}\right\} \tag{12}$$

where, T_{max} is the maximum torque, T_{min} refers to the minimum torque.

During regenerative condition of EVs, the current flows in and out from the battery frequently. However, the large current fluctuation is much harmful to battery because it can directly shorten battery lifetime. Therefore, the current fluctuation I_r should be reduced. In this paper, the current smoothness I_s is considered to assess current fluctuation, which is expressed as

$$I_s = \frac{1}{I_r} = \frac{I_{ave}}{I_{max} - I_{min}} \tag{13}$$

where, I_{max} and I_{min} are the maximum and minimum values of bus current, respectively; I_{ave} is the average bus current.

The output generated power, torque smoothness, and current smoothness defined above are selected as optimization objectives to improve the driving range, braking comfort, and battery lifetime for EVs, respectively. And the values of these objectives should be expected to be higher.

B. MULTI-OBJECTIVE OPTIMIZATION

In order to improve the comprehensive performance of EVs under regenerative braking condition and increase the lifetime of battery, a multi-objective synchronization optimization strategy is proposed in this paper. According to the three objectives defined above, the objective function with three weight factors is developed and expressed as

$$K\left(\theta_{on}, \theta_{off}\right) = \omega_1 \frac{P_{out}}{P_{max}} + \omega_2 \frac{\tau}{\tau_{max}} + \omega_3 \frac{I_s}{I_{s\,max}} \tag{14}$$

where, P_{max}, τ_{max}, and, I_{smax} are the maximum values of all sampled data obtained from output generated power, torque smoothness, and current smoothness, respectively; ω_1, ω_2, and ω_3 are the weight factors of the three objectives.

Therefore, the optimization function is determined based on the objective function, which is expressed as

$$K_{\text{opt}}\left(\theta_{on}, \theta_{off}\right) = \max\left\{\omega_1 \frac{P_{out}}{P_{max}} + \omega_2 \frac{\tau}{\tau_{max}} + \omega_3 \frac{I_s}{I_{s\,max}}\right\} \tag{15}$$

Considering the requirements of EVs, the output generated power of the SRG, which is the one of most important characteristics for increasing driving range, is more significant than torque ripple and current fluctuation. In addition, the importance of torque ripple and current fluctuation, which are implying vehicle comfort and battery lifetime, are almost the same. Hence, the three weight factors of the objective function are defined as 0.5, 0.25, and 0.25 in this paper, based on the comprehensive consideration. It should be noted that the weight factors could be selected according to different optimization requirements. Furthermore, the simulation for the SRG drive system is carried out under each available combination between turn-on and turn-off angles such that the database of output generated power, torque smoothness, and current smoothness can be established under various speeds and reference currents. Then the index K can be calculated by equation (14) and the optimized value can also be solved by equation (15).

According to the optimization function defined in this paper, the multi-objective optimization framework of the SRG drive system is designed and shown in Fig. 10. According to Fig. 6 and Fig. 10, when SRG works at low speed, the comprehensive index K with various speeds and reference currents is calculated and obtained by means of equation (14). As a result, the optimal switch angles can be obtained by equation (15) under the constraints of rotor speeds and reference currents, which are shown in Fig. 11. Similarly, when SRG works at high speed, the comprehensive index can be built under various speeds, and the optimal switch angles can be acquired at various rotor speeds as shown in Fig. 12.

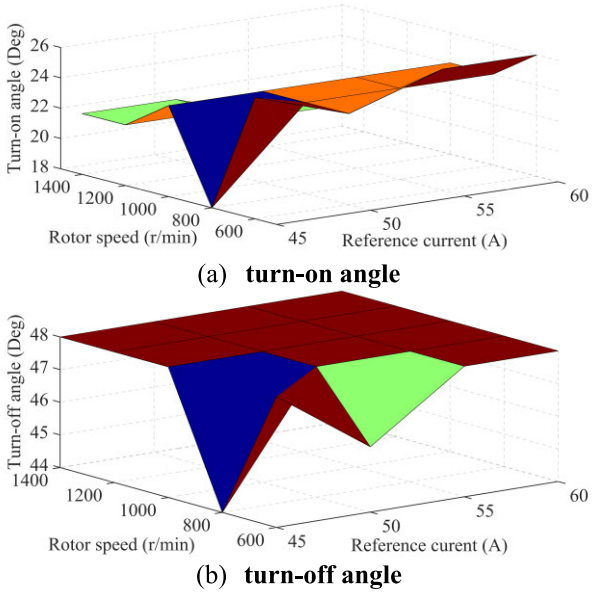

(a) **turn-on angle**

(b) **turn-off angle**

FIGURE 11. The optimized angles at low speed.

It can be seen from Fig. 11 that the optimal turn-on angle tends to increase from 22° to 26° as the rotor speed decreases, and decrease with the increase of reference current. The optimal turn-off angle is basically constant at 48°, except that the angle is 44° under condition of 800 r/min and 45 A. For high speed in Fig. 12, the optimal turn-on angle is almost stable at 18°, except that the angle is 20° at 2600 r/min. The optimal turn-off angle varies between 40° and 44°, indefinitely.

IV. SRG OPTIMIZIATION CONTROLLER

In order to attain the smooth transition between low and high speed, the control strategies based on low and high speed should be jointed to achieve better control within wide speed range. Thus, as shown in Fig. 13, a switching system is designed between two control modes, which can effectively reduce the switching frequency if the speed of SRG is varying near the base speed [20].

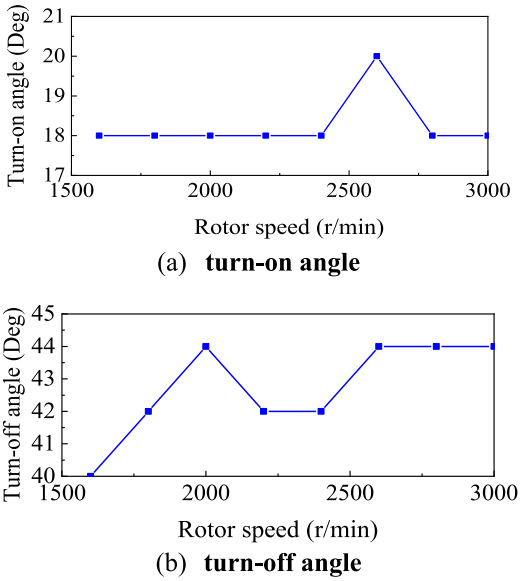

FIGURE 12. The optimized angles at high speed.

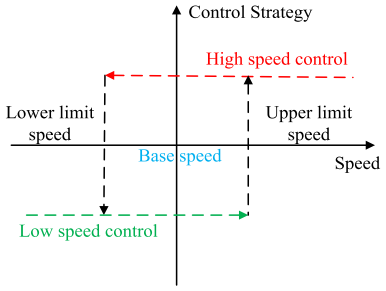

FIGURE 13. Switching system.

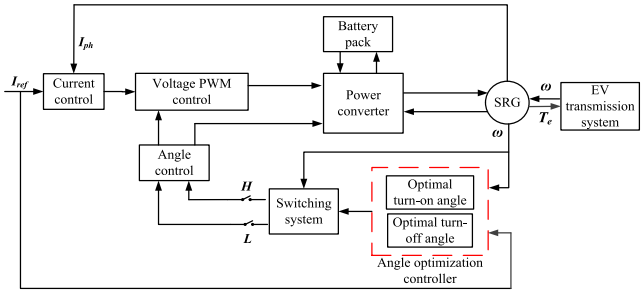

FIGURE 14. SRG optimization control system.

The angle optimization controller is designed based on the results from multi-objective optimization. Combining switching system and angle optimization controller, SRG optimization control system is established as shown in Fig. 14. The optimal switch angle is obtained based on angle optimization controller by the real-time rotor speed and reference current. Furthermore, the switching system can realize conversion of different control modes according to the rotor speed.

V. COMPARISON AND ANALYSIS OF RESULTS

In order to obtain the influence of multi-objective optimization control strategy on the dynamic performance of SRG, multi-objective optimization and output power optimization strategy are compared and analyzed in this paper. Comparing to the multi-objective optimization strategy, the output power is considered singly for the output power optimization strategy. Namely, the three weight factors of the objective function in equation (15) are fixed to 1, 0, and 0, respectively.

Considering the output generated power, an output power factor K_{Pout} calculated by means of optimized output power and maximum power is expressed as equation (16). Similarly, the torque smoothness factor K_τ and current smoothness factor K_{Is} are also defined as shown in equation (16).

$$\begin{cases} K_{P_{out}} = \dfrac{P_{opt}}{P_{max}} \\ K_\tau = \dfrac{\tau_{opt}}{\tau_{max}} \\ K_{I_s} = \dfrac{I_{sopt}}{I_{s\,max}} \end{cases} \tag{16}$$

From equation (16), it can be analyzed that the closer the three factor values reach to 1, the more obvious the improvement of the overall dynamic performance of the SRG.

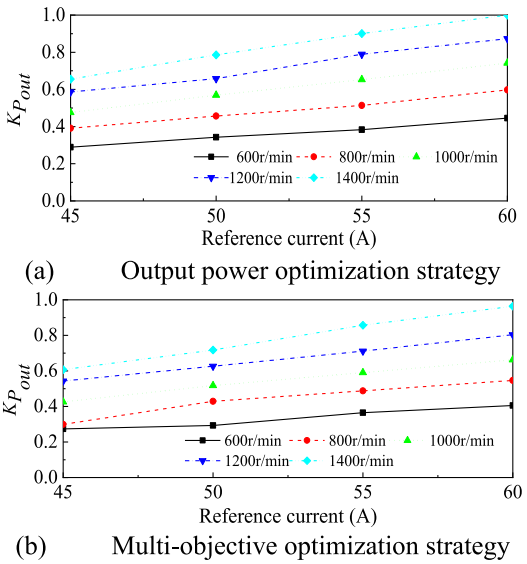

FIGURE 15. Output power factor at low speed.

A. SRG DYNAMIC CHARACTERISTIC

When SRG is running at low speed, the results from two optimization strategies are compared and analyzed by means of three factors defined above, as shown in Fig. 15 to Fig. 17. Considering the positive proportion relationship between the reference current I_{ref} and the average torque T_a. The reference current I_{ref}, which is one of the input control parameters for SRG drive system in Fig. 14, is selected as the horizontal axis to compare the two control strategies. It can be seen

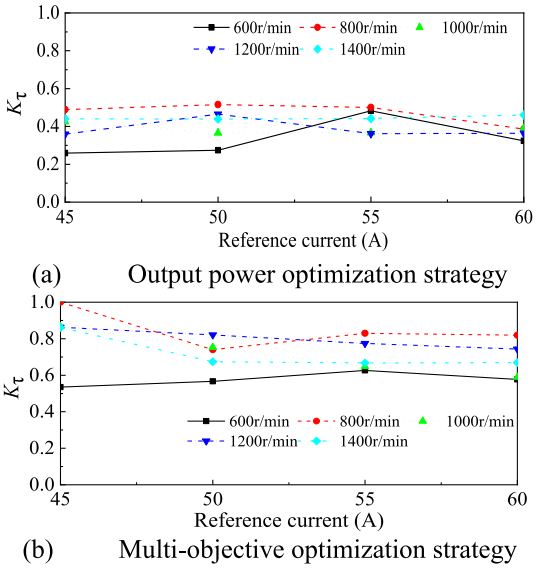

FIGURE 16. Torque smoothness factor at low speed.

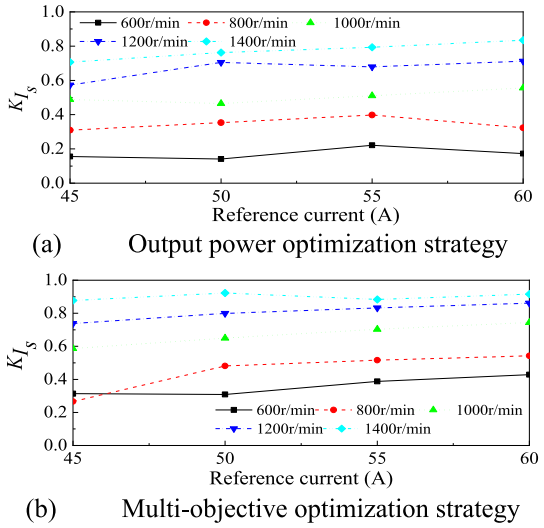

FIGURE 17. Current smoothness factor at low speed.

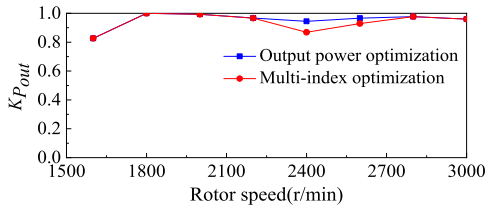

FIGURE 18. Output power factor at high speed.

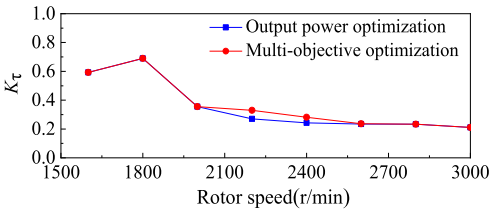

FIGURE 19. Torque smoothness factor at high speed.

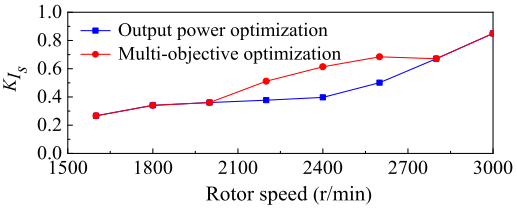

FIGURE 20. Current smoothness factor at high speed.

from Fig. 15 that the output power optimization strategy can achieve the maximum output power. The output power of the multi-objective optimization strategy will be slightly reduced under the same conditions. However, the multi-objective optimization strategy can also significantly improve the output generated power, and meeting the requirements of increasing the driving range of EVs driven by SRM. Fig. 16 presents that the torque smoothness factor varies within a small value range of 0.25 to 0.52 under the output power optimization strategy. The results show that the output power optimization strategy can't improve the torque smoothness such that the torque ripple is larger. Nevertheless, the values of the torque smoothness factor are 0.53 to 1 under the multi-objective optimization strategy, which is greatly improved by comparing with that under output power optimization strategy. It demonstrates that the strategy can prominently improve the torque smoothness and effectively reduce the torque ripple, ensuring the braking smoothness and improving the braking comfort of EVs. Fig. 17 shows that the current smoothness factor varies between 0.14 and 0.84 under the output power optimization strategy. And the factor is relatively higher under the multi-objective optimization strategy than that under power optimization strategy, which varies within a range of 0.26 to 0.93. Thus, comparing with output power optimization strategy, the multi-objective optimization strategy dramatically reduces the current fluctuation and achieves the purpose of extending the battery lifetime. Furthermore, the analysis of the above results shows that the three optimization weight factors defined are correct and reasonable.

The results obtained from two control strategies are also compared and analyzed by three factors at high speed of SRG, which are shown in Fig. 18 to Fig. 20. It can be seen from Fig. 18 that the output power optimization strategy can maximize the output generated power at high speed. Although the output power factor under the multi-objective optimization control strategy decreases slightly in the range of 2200 to 2800 r/min, the factor values are all above 0.8, indicating that the multi-objective optimization strategy can also achieve high efficiency for charging the battery to increase the driving range. As show in Fig. 19, the multi-objective optimization strategy improves the torque smoothness factor under speeds from 2000 to 2600 r/min, demonstrating that this strategy can increase the torque smoothness and reduce

torque ripple of SRG at high speed. Besides, the current smoothness factor can be improved under the multi-objective optimization control strategy as shown in Fig. 20, comparing with that under the output power optimization strategy. As a result, the multi-objective optimization control strategy can reduce the current fluctuation of SRG and extend the lifetime of the battery. Besides, from another aspect, it reflects the correctness of the definition of the optimization weight factor by the above analysis of the results.

Considering the results under both speed conditions, the output power optimization strategy can well improve the power generation by SRG, although the values of the output power factor reduce slightly under some conditions by comparing to output power optimization strategy. Obviously, the multi-objective optimization strategy is greatly better at improving torque ripple and current fluctuation than the power optimization strategy. On the whole, the multi-objective optimization control strategy can achieve a good balance among the output generated power, torque smoothness, and current smoothness through weight factors, which greatly improves the operating performance of SRG at high and low speed. Furthermore, it can significantly promote the comprehensive performance of EVs under regenerative braking condition and enhance the battery lifetime.

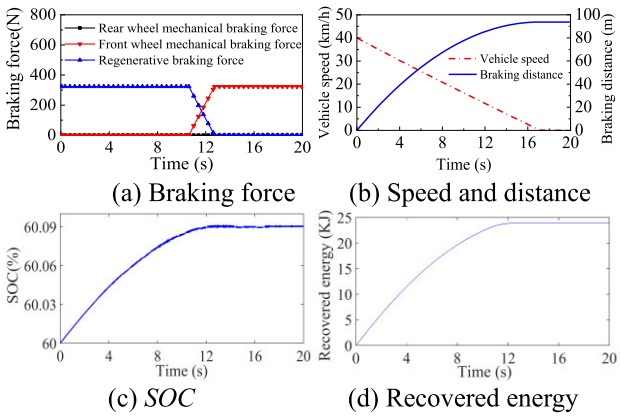

FIGURE 21. Simulation results under low-intensity braking for z = 0.05.

B. VEHICLE DYNAMIC CHARACTERISTICS

To evaluate the dynamic characteristics of the vehicle and the performance of the braking force distribution controller (BFDC) under the multi-objective optimization strategy, the low-intensity, medium-intensity, and emergency braking conditions are simulated and analyzed. The initial vehicle speed is set as 40 km/h, and the initial *SOC* of the battery is 0.6. The braking intensity is 0.05 and 0.1 under low braking condition, while the braking intensity of medium and emergency braking conditions are 0.4 and 0.7, respectively. In order to verify the performance of regenerative braking system for EVs, the braking force, vehicle speed and braking distance, battery *SOC*, and recovered energy are evaluated and analyzed, which is shown in Fig. 21 to Fig. 24.

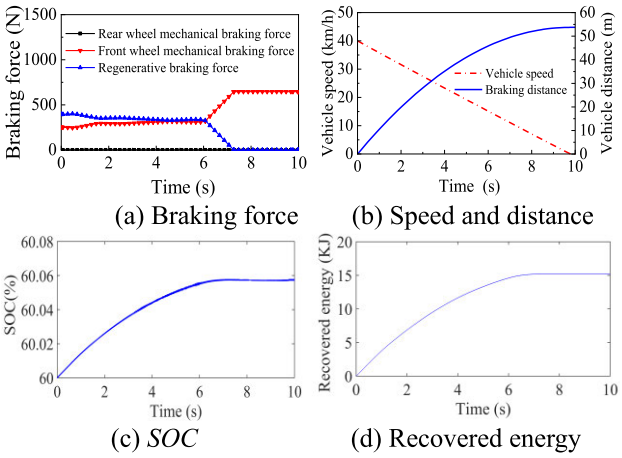

FIGURE 22. Simulation results under low-intensity braking for z = 0.1.

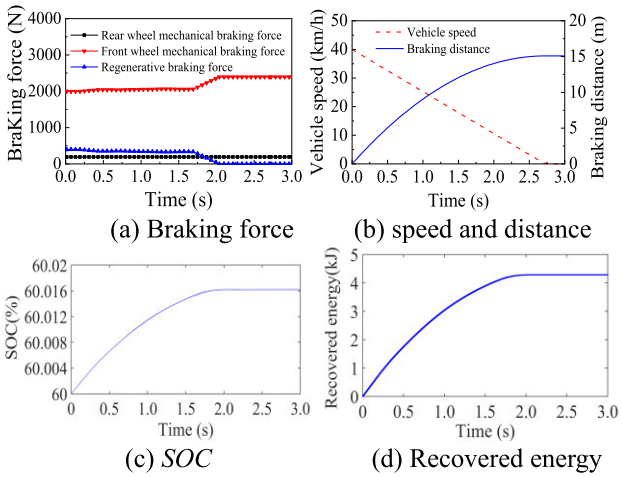

FIGURE 23. Simulation results under medium-intensity braking for z = 0.4.

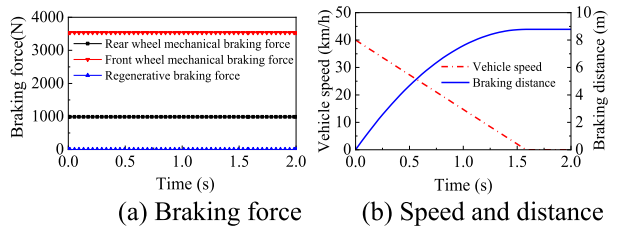

FIGURE 24. Simulation results under emergency braking for z = 0.7.

As shown in Fig. 21 and 22, the braking force is provided only by the front wheels under the condition of low-intensity braking. The braking force required by the front wheels are all provided through the motor under braking intensity of 0.05. In this case, the growth rate of *SOC* is 0.15%, the recovered energy increases by 24 kJ, and the braking distance is 93 m. When the braking intensity is 0.1, the braking force required by the front wheels is provided through the regenerative and mechanical braking system. The *SOC* energy growth rate is 0.1% and recovered energy increases by 15 kJ.

Meanwhile, the braking distance is 54 m. Therefore, the BFDC combined with optimized SRG control system can well guarantee the recovered braking energy and growing *SOC* under the low-intensity braking conditions. Fig. 23 presents the results from medium-intensity braking condition with a braking intensity of 0.4. In this case, the braking force required is jointly provided by the front and rear wheels such that the proportion of regenerative braking force is reduced. In addition, the *SOC* growth rate is 0.026%, and the recovered energy increases by 4.2 kJ. The growth rates of *SOC* and recovered energy under medium-intensity braking is much smaller than those under low-intensity braking, because of participation of mechanical braking system. But the speed of the vehicle with medium-intensity braking is reduced rapidly to ensure that the EV can stop within a short distance to meet the requirements of braking safety. It can be seen from Fig. 24 that the braking forces of front and rear wheels are only provided by mechanical braking system, without participating of regenerative braking system. Besides, the speed of the vehicle drops rapidly such that the EV can stop at a very short distance. Therefore, the BFDC designed in this paper can ensure the safety performance of EVs under condition of emergency braking.

To further compare the performance of braking system for EVs under the two SRG optimization strategies, the initial speed of 60km/h, 40km/h, and 20km/h are selected to simulate under various braking intensity, as shown in Fig. 25 to 27.

In order to numerically evaluate the differences between two strategies, the braking energy recovery efficiency η_{reg} indicating regenerative power is defined in this paper on the performance of braking system for EVs, which can be expressed as equation (17).

$$\eta_{reg} = \frac{E_{reg}}{E_{bk}} \times 100\% = \frac{\int_0^t UIdt}{\frac{1}{2}mu^2 - \int_0^t fmgudt - \int_0^t \frac{C_D A}{21.15} \cdot (3.6u)^2 \cdot udt} \times 100\% \tag{17}$$

where, E_{reg} represents the actual energy recovered, E_{bk} means maximum recoverable energy, U denotes battery voltage, I is battery current, and t is the deceleration time of the EVs.

Similarly, the longitudinal braking smoothness a_s is defined to assess the braking comfort performance of EVs, which is different from the previously defined torque smoothness optimizing the SRG drive system and the a_s is expressed as

$$a_s = \frac{1}{a_r} = \frac{1}{\left[\frac{1}{t}\int_0^t (a(t) - a_{ave})^2\, dt\right]^{1/2}} \tag{18}$$

where, a_r is defined as longitudinal braking impact degree, a_{ave} represents average deceleration, and $a(t)$ is braking deceleration.

To evaluate the influences of the two strategies on battery lifetime, c_r is defined by the standard deviation of the bus current, the battery lifetime coefficient c_s is defined by the reciprocal of c_r and expressed as

$$c_s = \frac{1}{c_r} = \frac{1}{\left[\frac{1}{t}\int_0^t (i(t) - i_{ave})^2\, dt\right]^{1/2}} \tag{19}$$

where, c_r is defined as the fluctuation degree of bus current, i_{ave} represents average bus current, and $i(t)$ denotes bus current.

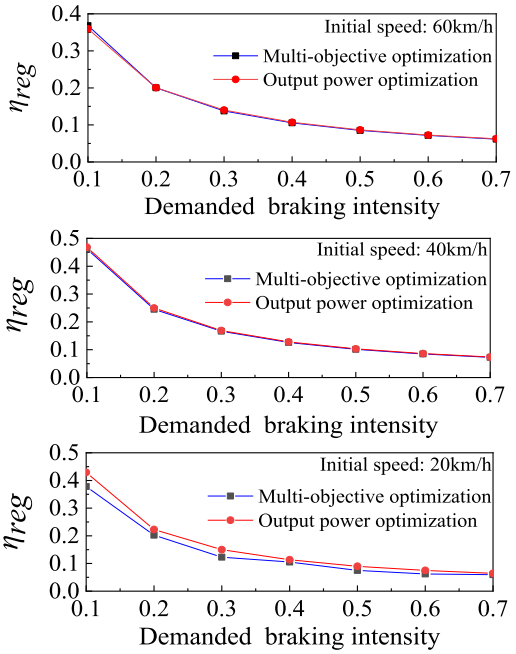

FIGURE 25. Braking energy recovery efficiency.

It can be concluded from Fig. 25 that the energy recovery efficiency of the braking system under the multi-objective optimization strategy is slightly less than that of the output power optimization strategy. Furthermore, the energy recovery efficiency is basically the same at initial speed of 60km/h under the two control strategies. When the demanded braking intensity is 0.1, compared with the output power optimization strategy, the maximum reduction in energy recovery efficiency occurs at the initial braking speed of 40km/h and 20km/h under the multi-objective control strategies, besides, the reduction rates are 1.34% and 7.24%. As shown in Fig. 26, the longitudinal braking smoothness under the multi-objective optimization strategy is significantly higher than that under output power optimization strategy. For initial speed of 60km/h, the longitudinal braking smoothness is basically 9.6 under the multi-objective optimization strategy, while the braking smoothness is maintained at 8.5 under output power optimization strategy. When the demanded braking intensity is 0.5, the longitudinal braking smoothness increases the most in the multi-objective optimization strategy compared with the output power optimization

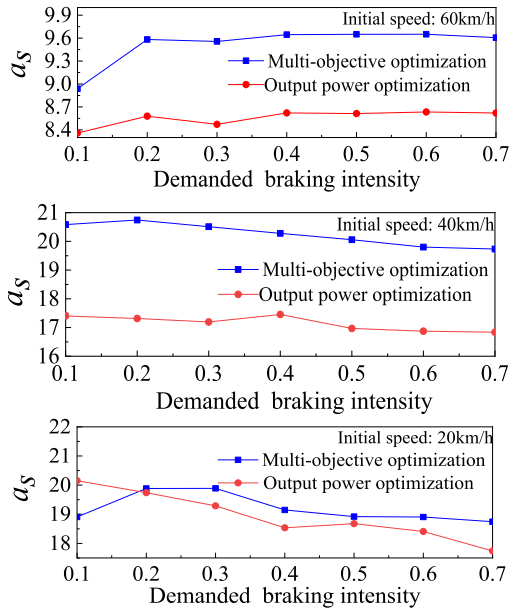

FIGURE 26. Braking smoothness.

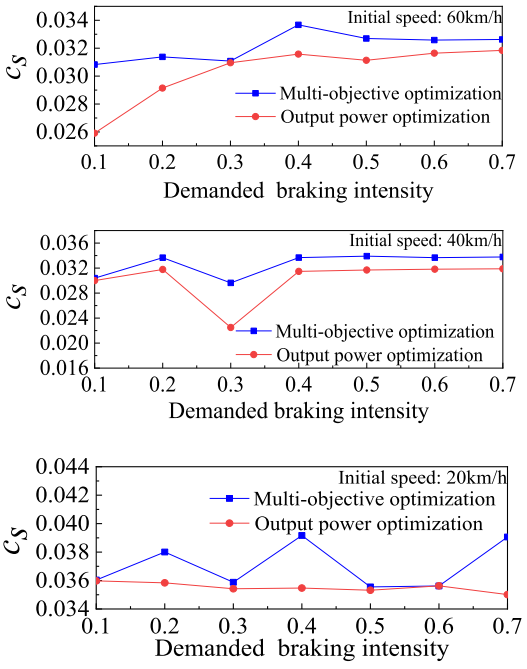

FIGURE 27. Battery lifetime coefficient.

strategy, and the increase is 12.03%. Similarly, compared with the output power optimization strategy, the increase value of the longitudinal brake smoothness is from 2.83 to 3.43 under the multi-objective optimization strategy for initial speed of 40km/h, which increased the maximum by 19.8%, meanwhile, the maximum increase is 3.31% at the initial speed of 20km/h. In addition, the battery lifetime coefficient under the multi-objective optimization strategy is also greatly higher than that under the output power optimization strategy, especially at initial speed of 60 and 40km/h from figure 27. Also, compared with the output power optimization strategy, the battery lifetime coefficient growth rates are 18.97%, 5.93%, and 6.05% under the multi-objective optimization strategy at initial speeds of 60km / h, 40km/h, and 20km/h, respectively. Therefore, comparing to the output power optimization strategy for SRG drive system, it can be also observed that the braking system under the multi-objective optimization strategy can effectively increase the vehicle braking comfort and improve battery lifetime without decreasing recovery energy.

VI. CONCLUSION

In this paper, the braking system model of the front drive vehicle driven by a four-phase 8/6 SRM was established, including mechanic braking system, SRG drive system model, and partition braking force distribution system. Then, a regenerative braking control strategy was proposed to improve braking performance and regenerative energy of the vehicle based on multi-objective optimization of SRG drive system, where output generated power, torque smoothness, and current smoothness were selected as optimization objectives to improve the driving range, braking comfort, and battery lifetime, respectively. Combing with the SRG optimization drive system, the braking system of EV was built and analyzed by various braking conditions. To separately consider the performance of SRG drive system and vehicle braking system, the simulations were carried out and compared based on the two optimization strategies. The comparison results show that the vehicle braking system with the SRG drive system under multi-objective optimization strategy can effectively reduce torque ripple and current fluctuation without obviously decreasing recovered braking energy, comparing to the output power optimization strategy. Therefore, the proposed regenerative braking control strategy based on optimization of SRG drive system can achieve a comprehensive balance among braking comfort, battery lifetime, and driving range of EVs.

REFERENCES

[1] Y. Huang, H. Wang, A. Khajepour, H. He, and J. Ji, "Model predictive control power management strategies for HEVs: A review," *J. Power Sources*, vol. 341, pp. 91–106, Feb. 2017.

[2] I. Boldea, L. N. Tutelea, L. Parsa, and D. Dorrell, "Automotive electric propulsion systems with reduced or no permanent magnets: An overview," *IEEE Trans. Ind. Electron.*, vol. 61, no. 10, pp. 5696–5711, Oct. 2014.

[3] X. Tang, W. Yang, X. Hu, and D. Zhang, "A novel simplified model for torsional vibration analysis of a series-parallel hybrid electric vehicle," *Mech. Syst. Signal Process.*, vol. 85, pp. 329–338, Feb. 2017.

[4] C. Sikder, I. Husain, and Y. Sozer, "Switched reluctance generator control for optimal power generation with current regulation," *IEEE Trans. Ind. Appl.*, vol. 50, no. 1, pp. 307–316, Jan. 2014.

[5] K. M. Rahman, B. Fahimi, G. Suresh, A. V. Rajarathnam, and M. Ehsani, "Advantages of switched reluctance motor applications to EV and HEV: Design and control issues," *IEEE Trans. Ind. Appl.*, vol. 36, no. 1, pp. 111–121, Jan. 2000.

[6] N. H. Saad, A. A. El-Sattar, and M. E. Metally, "Artificial neural controller for torque ripple control and maximum power extraction for wind system driven by switched reluctance generator," *Ain Shams Eng. J.*, vol. 9, no. 4, pp. 2255–2264, Dec. 2018.

[7] W. Ding, G. Liu, and P. Li, "A hybrid control strategy of hybrid-excitation switched reluctance motor for torque ripple reduction and constant power extension," *IEEE Trans. Ind. Electron.*, vol. 67, no. 1, pp. 38–48, Jan. 2020.
[8] Y. Zhu, C. Yang, G. Zhao, and D. Wang, "Optimization of switched reluctance motor drive system in electric vehicles application. journal of motor and control," *Electr. Mach. Contrl.*, vol. 22, no. 10, pp. 25–34, Sep. 2018.
[9] M. M. Namazi, S. M. Saghaiannejad, A. Rashidi, and J. W. Ahn, "Maximum power recovery of regenerative braking in electric vehicles based on switched reluctance drive," *J. Electr. Eng. Technol.*, vol. 13, no. 2, pp. 800–811, Mar. 2018.
[10] H. Yahia, R. Dhifaoui, and N. Liouane, "Differential evolution method-based output power optimisation of switched reluctance generator for wind turbine applications," *IET Renew. Power Gener.*, vol. 8, no. 7, pp. 795–806, Sep. 2014.
[11] J. Z. Zhang, C. lv, and Y. T. Li, "Hybrid propulsion and hybrid braking technologies of electrified vehicles: Status and prospect," *J. Automot. Saf. Energy*, vol. 5, no. 3, pp. 209–223, Mar. 2014.
[12] Y. Qin, X. Tang, T. Jia, Z. Duan, J. Zhang, Y. Li, and L. Zheng, "Noise and vibration suppression in hybrid electric vehicles: State of the art and challenges," *Renew. Sustain. Energy Rev.*, vol. 124, May 2020, Art. no. 109782.
[13] T. Liu, X. Tang, H. Wang, H. Yu, and X. Hu, "Adaptive hierarchical energy management design for a plug-in hybrid electric vehicle," *IEEE Trans. Veh. Technol.*, vol. 68, no. 12, pp. 11513–11522, Dec. 2019.
[14] X. Tang, X. Hu, W. Yang, and H. Yu, "Novel torsional vibration modeling and assessment of a power-split hybrid electric vehicle equipped with a dual-mass flywheel," *IEEE Trans. Veh. Technol.*, vol. 67, no. 3, pp. 1990–2000, Mar. 2018.
[15] W. Li, H. Du, and W. Li, "Driver intention based coordinate control of regenerative and plugging braking for electric vehicles with in-wheel PMSMs," *IET Intell. Transp. Syst.*, vol. 12, no. 10, pp. 1300–1311, Dec. 2018.
[16] J. Zhang, W. Sun, Z. Liu, and M. Zeng, "Comfort braking control for brake-by-wire vehicles," *Mech. Syst. Signal Process.*, vol. 133, Nov. 2019, Art. no. 106255.
[17] Y. Yuan, J. Zhang, Y. Li, and C. Li, "A novel regenerative electrohydraulic brake system: Development and Hardware-in-Loop tests," *IEEE Trans. Veh. Technol.*, vol. 67, no. 12, pp. 11440–11452, Dec. 2018.
[18] S. Zhang, K. Gao, Y. Zhou, C. Zhu, Y. Xiao, and Z. Huang, "Regenerative braking control strategy of electric vehicle based on composite power supply," in *Proc. 37th Chin. Control Conf. (CCC)*, Wuhan, China, Jul. 2018, pp. 7588–7593.
[19] Z. Junzhi, L. Yutong, L. Chen, and Y. Ye, "New regenerative braking control strategy for rear-driven electrified minivans," *Energy Convers. Manage.*, vol. 82, pp. 135–145, Jun. 2014.
[20] X. Nian, F. Peng, and H. Zhang, "Regenerative braking system of electric vehicle driven by brushless DC motor," *IEEE Trans. Ind. Electron.*, vol. 61, no. 10, pp. 5798–5808, Oct. 2014.
[21] C. Nanda Kumar and S. C. Subramanian, "Brake force sharing to improve lateral stability while regenerative braking in a turn," *Proc. Inst. Mech. Eng., D, J. Automobile Eng.*, vol. 233, no. 3, pp. 531–547, Feb. 2019.
[22] T. A. D. S. Barros, P. J. D. S. Neto, P. S. N. Filho, A. B. Moreira, and E. R. Filho, "An approach for switched reluctance generator in a wind generation system with a wide range of operation speed," *IEEE Trans. Power Electron.*, vol. 32, no. 11, pp. 8277–8292, Nov. 2017.
[23] R. Mendes, M. Calado, and S. Mariano, "Maximum power point tracking for a point absorber device with a tubular linear switched reluctance generator," *Energies*, vol. 11, no. 9, p. 2192, 2018.
[24] E. Roshandel, M. M. Namazi, A. Rashidi, S. M. Saghaian-Nejad, and J.-W. Ahn, "SSC strategy for SRG to achieve maximum power with minimum current ripple in battery charging," *IET Electr. Power Appl.*, vol. 11, no. 7, pp. 1205–1213, Aug. 2017.
[25] S. Narla, Y. Sozer, and I. Husain, "Switched reluctance generator controls for optimal power generation and battery charging," *IEEE Trans. Ind. Appl.*, vol. 48, no. 5, pp. 1452–1459, Sep. 2012.
[26] F. Yi and W. Cai, "Modeling, control and seamless transition of bi-directional battery-driven switched reluctance Motor/Generator drive based on integrated multiport power converter for electric vehicle applications," *IEEE Trans. Power Electron.*, vol. 31, no. 10, pp. 7099–7111, Oct. 2016.
[27] K. Kannan and S. Sutha, "PI-CCC based minimization of torque ripple in switched reluctance generator using MATLAB/SIMULINK," in *Proc. 4th Int. Power Eng. Optim. Conf. (PEOCO)*, Shah Alam, Malaysia, Jun. 2010, pp. 522–527.
[28] H.-U. Shin, K. Park, and K.-B. Lee, "A non-unity torque sharing function for torque ripple minimization of switched reluctance generators in wind power systems," *Energies*, vol. 8, no. 10, pp. 11685–11701, 2015.
[29] K. V. Subramaniyam and S. C. Subramanian, "Analysis of cornering response and stability of electrified heavy commercial road vehicles with regenerative braking," *Proc. Inst. Mech. Eng., D, J. Automobile Eng.*, vol. 234, no. 6, pp. 1672–1689, May 2020.
[30] E. Mehrdad, G. Yimin, and E. Ali, "Modern electric hybrid electric, and fuel cell vehicles: Fundamentals, theory, and design," *IEEE Ind. Electron. Mag.*, vol. 4, no. 1, p. 75, Mar. 2010.
[31] S. Li, B. Yu, and X. Feng, "Research on braking energy recovery strategy of electric vehicle based on ECE regulation and i curve," *Sci. Prog.*, vol. 103, no. 1, Jan. 2020, Art. no. 003685041987776.
[32] J. Nadeau, P. Micheau, and M. Boisvert, "Collaborative control of a dual electro-hydraulic regenerative brake system for a rear-wheel-drive electric vehicle," *Proc. Inst. Mech. Eng., D, J. Automobile Eng.*, vol. 233, no. 4, pp. 1035–1046, Mar. 2019.
[33] D. Wu, B. Zhu, D. Tan, N. Zhang, and J. Gu, "Multi-objective optimization strategy of adaptive cruise control considering regenerative energy," *Proc. Inst. Mech. Eng., D, J. Automobile Eng.*, vol. 233, no. 14, pp. 3630–3645, Dec. 2019.
[34] D.-W. Choi, S.-I. Byun, and Y.-H. Cho, "A study on the maximum power control method of switched reluctance generator for wind turbine," *IEEE Trans. Magn.*, vol. 50, no. 1, pp. 1–4, Jan. 2014.
[35] Y. Zhu, W. Wei, C. Yang, and Y. Zhang, "Multi-objective optimisation design of two-phase excitation switched reluctance motor for electric vehicles," *IET Electr. Power Appl.*, vol. 12, no. 7, pp. 929–937, Aug. 2018.
[36] Y. Zhu, C. Yang, Y. Yue, C. Zhao, and Y. Zhang, "Development and analysis of a two-phase excitation switched reluctance motor with novel winding distribution used in electric vehicles," *J. Electr. Eng. Technol.*, vol. 13, no. 6, pp. 2364–2375, Nov. 2018.
[37] Q. Wang, H. Chen, and R. Zhao, "Double-loop control strategy for SRGs," *IET Electr. Power Appl.*, vol. 11, no. 1, pp. 29–40, Jan. 2017.
[38] X. D. Xue, K. W. E. Cheng, J. K. Lin, Z. Zhang, K. F. Luk, T. W. Ng, and N. C. Cheung, "Optimal control method of motoring operation for SRM drives in electric vehicles," *IEEE Trans. Veh. Technol.*, vol. 59, no. 3, pp. 1191–1204, Mar. 2010.

YUEYING ZHU (Member, IEEE) was born in Shandong, China, in 1982. He received the B.Sc., M.Sc., and Ph.D. degrees in mechanical engineering from the Harbin Institute of Technology, China, in 2006, 2008, and 2011, respectively. From 2018 to 2019, he was with the University of Waterloo, Canada, as a Visiting Scholar. He is currently an Associate Professor with the College of Mechanical Engineering, Tianjin University of Science and Technology. His research interests include electric vehicle drive control, in-wheel motor control, and switched reluctance motor control.

HAO WU was born in Anhui, China, in 1994. He received the B.S. degree in vehicle engineering from the Tianjin University of Science and Technology in 2018, where he is currently pursuing the M.Sc. degree. His main research interests are in the field of regenerative braking control of electric vehicles and SRG control.

JUNXIA ZHANG was born in Shanxi, China, in 1968. She received the B.Sc. and M.Sc. degrees in mechanical engineering from the Taiyuan University of Technology, China, and the Ph.D. degree in mechanical engineering from Jilin University, China, in 1999. She is currently a Professor with the College of Mechanical Engineering, Tianjin University of Science and Technology. Her research interests include robotics design and control, man–machine engineering, and electric vehicle drive systems.